

# Bayesian automated posterior repartitioning for nested sampling

Xi Chen · Farhan Feroz · Michael Hobson

**Abstract** Priors in Bayesian analyses often encode informative domain knowledge that can be useful in making the inference process more efficient. Occasionally, however, priors may be unrepresentative of the parameter values for a given dataset, which can result in inefficient parameter space exploration, or even incorrect inferences, particularly for nested sampling (NS) algorithms. Simply broadening the prior in such cases may be inappropriate or impossible in some applications. Hence a previous solution of this problem, known as posterior repartitioning (PR), redefines the prior and likelihood while keeping their product fixed, so that the posterior inferences and evidence estimates remain unchanged, but the efficiency of the NS process is significantly increased. In its most practical form, PR raises the prior to some power  $\beta$ , which is introduced as an auxiliary variable that must be determined on a case-by-case basis, usually by lowering  $\beta$  from unity according to some pre-defined ‘annealing schedule’ until the resulting inferences converge to a consistent solution. We present here an alternative Bayesian ‘automated PR’ method, in which  $\beta$  is instead treated as a hyperparameter that is inferred from the data alongside the original parameters of the problem, and then marginalised over to obtain the final inference. We show through numerical examples that this approach provides a robust and efficient ‘hands-off’ solution to addressing the issue of unrepresentative priors in Bayesian inference using NS. Moreover, we show that for problems with representative priors the method has a negligible computational overhead relative to standard nesting sampling,

which suggests that it should be used in as a matter of course in all NS analyses.

**Keywords** Bayesian inference · automatic posterior repartitioning · nested sampling · unrepresentative prior

## 1 Introduction

In recent years, Monte Carlo sampling techniques have been widely used in Bayesian inference problems both for parameter estimation and model selection. Nested sampling (NS) (Skilling, 2006) is one such approach that can simultaneously produce samples from the posterior distribution and estimate the marginal likelihood (or evidence). The NS algorithm involves drawing samples from a pre-defined prior distribution, and then evaluating their corresponding likelihoods, which are dependent on some measurement (or forward) model and the observed data. In general, the observed data are fixed and the measurement model is defined by field experts, with little room for flexibility. In contrast, the prior that identifies the regions of interest in the parameter space is typically much more loosely determined and often defined using simple standard distributions, together occasionally with physical constraints on the parameters  $\theta$  of the problem under consideration.

As discussed in Chen et al (2018), the NS algorithm can become very inefficient, or even fail completely in extreme cases, if the likelihood for a given data set is concentrated far out in the wings of the assumed prior distribution. This problem can be particularly damaging in applications where one wishes to perform analyses on many thousands (or even millions) of different datasets, since those (typically few) datasets for which the prior is unrepresentative can absorb a large fraction of the computational resources.

X. Chen, F. Feroz, M. Hobson are with Cavendish Laboratory, Department of Physics, University of Cambridge, UK. CB3 0HE. E-mail: xc253@cam.ac.uk, f.feroz@mrao.cam.ac.uk, mph@mrao.cam.ac.uk.

The problem occurs because the NS algorithm begins by drawing a number of ‘live’ samples from the prior and at each subsequent iteration replaces the sample having the lowest likelihood with a sample again drawn from the prior but constrained to have a higher likelihood. Thus, as the iterations progress, the collection of live points gradually migrates from the prior to the peak of the likelihood. When the likelihood is concentrated very far out in the wings of the prior, this process can become very slow, even in the rare problems where one is able to draw each new sample from the constrained prior using standard methods (sometimes termed perfect nested sampling). In practice, this is usually not possible, so algorithms such as MultiNest (Feroz et al, 2009) and PolyChord (Handley et al, 2015) use other methods that may require several likelihood evaluations before a new sample is accepted. Depending on the method used, an unrepresentative prior can result in a significant drop in sampling efficiency, thereby increasing still further the required number of likelihood evaluations.

In extreme cases, the migration of live points in the NS process can be very slow, since over many iterations the live points will typically all lie in a region over which the likelihood is very small and flat. Indeed, in some such cases, the log-likelihoods of the set of live points may be indistinguishable to machine precision, so the lowest likelihood sample to be discarded will be chosen effectively at random and, in seeking a replacement sample that is drawn from the prior but having a larger likelihood, the algorithm is very unlikely to obtain a sample for which the likelihood value is genuinely larger to machine precision. These problems can result in the live point set migrating exceptionally slowly, or becoming essentially stuck, such that the algorithm (erroneously) terminates before reaching the main body of the likelihood and therefore fails to produce correct posterior samples or evidence estimates.

One may, of course, seek to improve the performance of NS in such cases by increasing the number of live points and/or adjusting the convergence criterion, so that many more NS iterations are performed, but there is no guarantee in any given problem that these measures will be sufficient to prevent premature convergence. Perhaps more useful is to ensure that there is a greater opportunity at each NS iteration of drawing candidate replacement points from regions of the parameter space where the likelihood is larger. This may be achieved in a variety of ways. In MultiNest, for example, one may reduce the `efr` parameter to enlarge the volume of the multi-ellipsoidal bound from which candidate replacement points are drawn. Alternatively, as in other NS implementations, one may draw candi-

date replacement points using either MCMC sampling (Feroz and Hobson, 2008) or slice-sampling (Handley et al, 2015) and increase the number of steps taken before a candidate point is chosen. All of these approaches may mitigate the problem to some degree in particular cases, but only at the cost of a simultaneous dramatic drop in sampling efficiency caused precisely by the changes made in obtaining candidate replacement points. Moreover, in more extreme cases, these measures may fail completely.

Aside from making changes to the implementation of the NS algorithm itself, one might consider simple solutions such as broadening the prior range in such cases, but this might not be appropriate or possible in real-world applications, for example when one wishes to assume a single standardised prior across the analysis of a large number of datasets for which the true values of the parameters of interest may vary.

Chen et al (2018) therefore proposed a posterior repartitioning (PR) method that circumvents the above difficulties. The PR method exploits the intrinsic degeneracy between the ‘effective’ likelihood and prior in the formulation of Bayesian inference problems. This is especially relevant for NS since it differs from other sampling methods by making use of the likelihood  $\mathcal{L}(\boldsymbol{\theta})$  and prior  $\pi(\boldsymbol{\theta})$  *separately* in its exploration of the parameter space, in that samples are drawn from the prior  $\pi(\boldsymbol{\theta})$  such that they satisfy some likelihood constraint  $\mathcal{L}(\boldsymbol{\theta}) > L_*$ . By contrast, Markov chain Monte Carlo (MCMC) sampling methods or genetic algorithm variants are typically blind to this separation<sup>1</sup>, and deal solely in terms of the product  $\mathcal{L}(\boldsymbol{\theta})\pi(\boldsymbol{\theta})$ , which is proportional to the posterior  $\mathcal{P}(\boldsymbol{\theta})$ . This difference provides an opportunity in the case of NS to ‘repartition’ the product  $\mathcal{L}(\boldsymbol{\theta})\pi(\boldsymbol{\theta})$  by defining a new effective likelihood  $\tilde{\mathcal{L}}(\boldsymbol{\theta})$  and prior  $\tilde{\pi}(\boldsymbol{\theta})$  (which is typically ‘broader’ than the original prior), subject to the condition  $\tilde{\mathcal{L}}(\boldsymbol{\theta})\tilde{\pi}(\boldsymbol{\theta}) = \mathcal{L}(\boldsymbol{\theta})\pi(\boldsymbol{\theta})$ , so that the (unnormalised) posterior remains unchanged. Thus, in principle, the inferences obtained are unaffected by the use of the PR method, but, as Chen et al (2018) demonstrated, the approach can yield significant improvements in sampling efficiency and also helps to avoid the convergence problems that can occur in extreme examples of unrepresentative priors.

In its most practical form, termed power posterior repartitioning (PPR), the effective prior  $\tilde{\pi}(\boldsymbol{\theta})$  is proportional simply to the original prior  $\pi(\boldsymbol{\theta})$  raised to some power  $\beta$ , which is introduced as an auxiliary variable. Although Chen et al (2018) demonstrated the effective-

<sup>1</sup> One exception is the propagation of multiple MCMC chains, for which it is often advantageous to draw the starting point of each chain independently from the prior distribution.

ness of this approach, one drawback of the method is that the auxiliary variable must be determined on a case-by-case basis, which is typically achieved by lowering  $\beta$  from unity outside the execution of NS algorithm according to some pre-defined ‘annealing schedule’, until the resulting inferences from successive NS runs converge to a statistically consistent solution for values below some (positive) threshold  $\beta \lesssim \beta_*$ . This approach lacks elegance and the repeated NS runs required can be computationally demanding. Moreover, the final inference is unavoidably conditioned on the value  $\beta_*$ .

In this paper, we therefore present an alternative Bayesian ‘automated’ PR (autoPR) method in which  $\beta$  is instead treated as a hyperparameter that is inferred from the data alongside the original parameters  $\theta$  of the problem, within a single execution of the NS algorithm. This furnishes samples from the joint posterior on  $(\theta, \beta)$  which may then be used straightforwardly to obtain either a final inference on  $\theta$  after marginalisation over  $\beta$ , or to determine the 1-dimensional marginal distribution of  $\beta$  by marginalising over  $\theta$ . The latter is useful in diagnosing the existence and severity of an unrepresentative prior for a given dataset, and hence for identifying ‘outlier’ datasets and in refining the inference problem for future analyses.

It is worth noting, however, that one may encounter even more extreme problems than those discussed above, where the likelihood for some dataset(s) is concentrated outside an assumed prior having compact support. From a probabilistic point of view, the prior in these problems has zero probability in the region of the likelihood distribution. This case, one might describe as an unsuitable prior, is not addressed by the PPR method, and is not considered here.

This paper is organised as follows. Section 2 briefly introduces the Bayesian inference and the NS algorithm. Section 3 outlines the original PR method and then describes the proposed Bayesian autoPR scheme. Section 4 demonstrates performance of the autoPR method in some numerical examples, and we present our conclusions in Section 5.

## 2 Bayesian inference using nested sampling

Bayesian inference (see e.g. MacKay 2003) provides a consistent framework for estimating unknown parameters  $\theta$  of some model by updating any prior knowledge of  $\theta$  using the observed data  $\mathcal{D}$  and an assumed measurement process. The complete inference is embodied in the posterior distribution of  $\theta$ , which can be

expressed using Bayes’ theorem as:

$$\Pr(\theta|\mathcal{D}, \mathcal{M}) = \frac{\Pr(\mathcal{D}|\theta, \mathcal{M}) \Pr(\theta|\mathcal{M})}{\Pr(\mathcal{D}|\mathcal{M})}, \quad (1)$$

where  $\mathcal{M}$  represents model (or hypothesis) assumption(s), and adopting a simplifying notation,  $\Pr(\theta|\mathcal{D}, \mathcal{M}) \equiv \mathcal{P}(\theta)$  is the *posterior* probability density,  $\Pr(\mathcal{D}|\theta, \mathcal{M}) \equiv \mathcal{L}(\theta)$  is the *likelihood*,  $\Pr(\theta|\mathcal{M}) \equiv \pi(\theta)$  is the *prior* probability density on  $\theta$  and  $\Pr(\mathcal{D}|\mathcal{M}) \equiv \mathcal{Z}$  is called the *evidence* (or marginal likelihood). We then have the simplified expression:

$$\mathcal{P}(\theta) = \frac{\mathcal{L}(\theta)\pi(\theta)}{\mathcal{Z}}, \quad (2)$$

in which the evidence is given by

$$\mathcal{Z} = \int_{\Psi} \mathcal{L}(\theta)\pi(\theta)d\theta, \quad (3)$$

where  $\Psi$  represents the prior space of  $\theta$ . The evidence  $\mathcal{Z}$  is often used for model selection. It is the average of the likelihood over the prior, considering every possible choice of  $\theta$ , and thus is not a function of the parameters  $\theta$ . The constant  $\mathcal{Z}$  is usually ignored in parameter estimation, since the posterior  $\mathcal{P}(\theta)$  is proportional to the product of likelihood  $\mathcal{L}(\theta)$  and prior  $\pi(\theta)$ .

Nested sampling (Skilling, 2006) explores the posterior distribution in a sequential manner using a fixed number of  $N_{\text{live}}$  ‘live samples’ of the parameters  $\theta$  at each iteration of the process. We note that the method has recently been extended to so-called dynamic nested sampling (Higson et al, 2018), which allows the number of live samples to vary as the NS iterations proceed, but we will not use this variant here. Pseudo-code for the standard NS algorithm is given in Algorithm 1.

In Algorithm 1,  $X_i$  denotes the expected fraction of the prior volume lying within the isolikelihood contour  $\mathcal{L}(\theta) = \mathcal{L}_i$  at iteration  $i$ . In general, the fractional prior volume  $X$  lying above some likelihood threshold  $\mathcal{L}^*$  is defined as

$$X(\mathcal{L}^*) = \int_{\mathcal{L}(\theta) > \mathcal{L}^*} \pi(\theta)d\theta, \quad (4)$$

where  $\mathcal{L}^*$  gradually rises from zero to the maximum of  $\mathcal{L}(\theta)$  as the NS iterations proceed. The NS algorithm provides an estimate of the evidence (3) by casting it as a one-dimensional integral with respect to fractional prior volume  $X$ :

$$\mathcal{Z} = \int_0^1 \mathcal{L}(X)dX, \quad (5)$$

subject to the existence of the inverse  $\mathcal{L}(X) \equiv X^{-1}(\mathcal{L})$ . Finally, `tol` denotes a pre-defined convergence criterion, which affects the number of NS iterations.

**Algorithm 1:** Nested sampling algorithm

---

```

// Nested sampling initialisation
1 At iteration  $i = 0$ :
2 Draw  $N_{\text{live}}$  samples  $\{\theta_n\}_{n=1}^{N_{\text{live}}}$  from prior  $\pi(\theta)$ .
3 Initialise evidence  $Z = 0$  and prior volume  $X_0 = 1$ .
// NS iterations
4 for  $i = 1, 2, \dots, I$  do
5   for  $n = 1, 2, \dots, N_{\text{live}}$  do
6     • Compute likelihood  $\mathcal{L}(\theta_n)$ .
7   end for
8   • Find the lowest likelihood and save in  $\mathcal{L}_i$ .
9   • Calculate weight  $w_i = \frac{1}{2}(X_{i-1} - X_{i+1})$ , where
      $X_i = \exp(-i/N_{\text{live}})$ 
10  • Increment  $Z$  by  $\mathcal{L}_i w_i$ .
11  • Draw new sample to replace one with likelihood
      $\mathcal{L}_i$ , subject to  $\mathcal{L}(\theta) > \mathcal{L}_i$ .
12  • Stop if  $\max\{\mathcal{L}(\theta_n)\}X_i < \text{tol} \times Z$ .
13 end for
14 Increment  $Z$  by  $\sum_{n=1}^{N_{\text{live}}} \mathcal{L}(\theta_n)X_I/N_{\text{live}}$ .
15 Assign the sample replaced at iteration  $i$  the
    importance weight  $p_i = \mathcal{L}_i w_i / Z$ .

```

---

Among the various implementations of the NS algorithm, two widely used packages are MultiNest (Feroz et al, 2009, 2013) and PolyChord (Handley et al, 2015). MultiNest draws the new sample at each iteration using rejection sampling from within a multi-ellipsoid bound approximation to the iso-likelihood surface defined by the discarded point; the bound is constructed from the live points present at that iteration. PolyChord draws the new sample at each iteration using a number of successive slice-sampling steps taken in random directions, which is particularly well suited to higher-dimensional problems. Please see Feroz et al (2009) and Handley et al (2015) for more details.

### 3 Bayesian automated posterior repartitioning

The possibility of improving the robustness and efficiency of NS by exploiting the intrinsic degeneracy between the ‘effective’ likelihood and prior in the formulation of Bayesian inference problems was first mentioned in Feroz et al (2009), and then further developed as the PR method by Chen et al (2018).

As mentioned in the Introduction, the central idea is to ‘repartition’ the product of the likelihood and prior, such that

$$\mathcal{L}(\theta)\pi(\theta) = \tilde{\mathcal{L}}(\theta)\tilde{\pi}(\theta), \quad (6)$$

where  $\tilde{\mathcal{L}}(\theta)$  and  $\tilde{\pi}(\theta)$  are the newly-defined effective (or modified) likelihood and prior, respectively. As a result, the (unnormalised) posterior remains unchanged and hence, in principle, any parameter inferences are unaffected. Moreover, if  $\tilde{\pi}(\theta)$  is normalised, then the

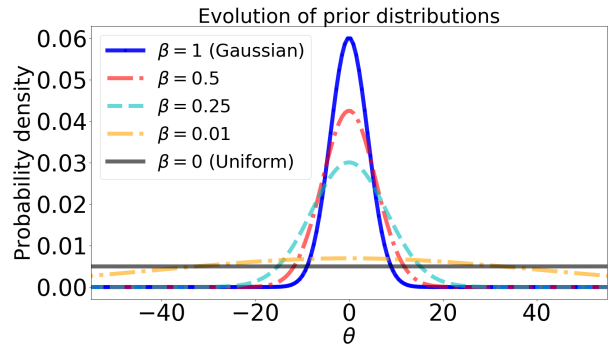


**Fig. 1** One-dimensional prior evolution for  $\beta \in [0, 1]$ . The original prior is a Gaussian distribution with  $\sigma_\pi = 4$  (truncated in the range  $[-50, 50]$ ) when  $\beta = 1$  (solid blue curve), and is an uniform distribution when  $\beta = 0$  (solid black curve). The remaining three curves correspond to  $\beta = 0.5$  (dot-dashed red curve), 0.25 (dashed light blue curve), 0.01 (dot-dashed yellow curve), respectively.

evidence also remains unchanged. In general,  $\tilde{\pi}(\theta)$  can be any tractable distribution. For example, there is no requirement for the modified prior to be centred at the same parameter value as the original prior. One could, therefore, choose a modified prior that broadens and/or shifts the original one, or a modified prior that has a completely different form from the original. In this generalised setting, however, the modified prior should at least be non-zero everywhere.

In practice, rather than introducing a completely new prior distribution into the problem, a convenient choice (termed power PR) is simply to take  $\tilde{\pi}(\theta)$  to be the original prior  $\pi(\theta)$  raised to some (real) power  $\beta$ , and then renormalised to unit volume, such that

$$\tilde{\pi}(\theta) = \frac{\pi(\theta)^\beta}{\mathcal{Z}_\pi(\beta)}, \quad (7)$$

$$\tilde{\mathcal{L}}(\theta) = \mathcal{L}(\theta)\pi(\theta)^{(1-\beta)}\mathcal{Z}_\pi(\beta), \quad (8)$$

where  $\beta \in [0, 1]$  and  $\mathcal{Z}_\pi(\beta) \equiv \int \pi(\theta)^\beta d\theta$  is the normalisation constant of the modified prior. By altering the value of  $\beta$ , the modified prior varies across a range of distributions between the original prior ( $\beta = 1$ ) and the uniform distribution ( $\beta = 0$ ). This is illustrated in Figure 1 for five specific  $\beta$  values in a one-dimensional case, where the original prior is a Gaussian with zero mean and standard deviation  $\sigma_\pi = 4$  and the normalisation depends on the assumed support  $[-50, 50]$  of the unknown parameter  $\theta$ . The  $\beta = 0$  limit clearly yields a uniform modified prior  $\tilde{\pi}(\theta) \sim \mathcal{U}(a, b)$ , which is an important special case in that it maximises the dispersion of the initial live point set across the prior space, but consequently can result in very inefficient sampling.

A clear drawback of the PR method, however, is that an appropriate value of the auxiliary variable  $\beta$  must be determined on a case-by-case basis, and this

can depend sensitively on the nature of the original prior and likelihood, as well as on the dimensionality of the problem under consideration. [Chen et al \(2018\)](#) therefore suggested an approach in which  $\beta$  is gradually lowered from unity (outside of the NS algorithm) according to some ‘annealing schedule’, until the resulting inferences from successive NS runs converge to a statistically consistent solution, which typically occurs for  $\beta$  values below some (positive) threshold,  $\beta \lesssim \beta_*$ . Although [Chen et al \(2018\)](#) demonstrated that this method is robust and effective, it has the disadvantages that there is a significant computational overhead associated with the multiple NS runs required and that the final inference of the parameters of interest  $\theta$  is conditioned on the adopted value  $\beta = \beta_*$ .

We therefore propose an alternative solution here, which we consider to be more elegant. In this approach,  $\beta$  is instead treated as a hyperparameter that is inferred in a Bayesian manner alongside the original parameters  $\theta$ , within a single run of the NS algorithm. This is straightforwardly achieved by defining the joint posterior

$$\tilde{\mathcal{P}}(\theta, \beta) \propto \tilde{\mathcal{L}}(\theta, \beta) \tilde{\pi}(\theta, \beta) = \tilde{\mathcal{L}}(\theta, \beta) \tilde{\pi}(\theta|\beta) \pi(\beta), \quad (9)$$

where  $\pi(\beta)$  denotes the assumed prior on the hyperparameter  $\beta$ , and  $\tilde{\pi}(\theta|\beta)$  and  $\tilde{\mathcal{L}}(\theta, \beta)$  have precisely the forms (7) and (8), respectively. Since  $\beta$  lies naturally in the range  $[0, 1]$ , we define  $\pi(\beta)$  to be the uniform prior over this interval, although other choices may be accommodated if there is a strong motivation to adopt an alternative form in a particular problem. From the relation (6) and (2), one sees that (by construction)

$$\tilde{\mathcal{P}}(\theta, \beta) \propto \mathcal{P}(\theta) \pi(\beta). \quad (10)$$

Moreover, the corresponding evidence is given by

$$\tilde{\mathcal{Z}} = \iint \tilde{\mathcal{L}}(\theta, \beta) \tilde{\pi}(\theta, \beta) d\theta d\beta \quad (11)$$

$$= \int \mathcal{L}(\theta) \pi(\theta) d\theta \int \pi(\beta) d\beta = \mathcal{Z}, \quad (12)$$

so that the proportionality in (10) can be replaced by an equality.

In principle, a single NS run thus provides samples from the full joint posterior distribution (10), which can be used straightforwardly to obtain inferences on the original parameters  $\theta$  after marginalisation over  $\beta$ , since

$$\tilde{\mathcal{P}}(\theta) = \int \tilde{\mathcal{P}}(\theta, \beta) d\beta = \int \mathcal{P}(\theta) \pi(\beta) d\beta = \mathcal{P}(\theta). \quad (13)$$

Hence, compared to the original PR method, the overall computational burden is much reduced and the final inference is not conditioned on a particular value of

$\beta$ . Conversely, one may instead marginalise over the original parameters  $\theta$ , which should in principle recover the prior on  $\beta$ , since

$$\tilde{\mathcal{P}}(\beta) = \int \tilde{\mathcal{P}}(\theta, \beta) d\theta = \int \mathcal{P}(\theta) \pi(\beta) d\theta = \pi(\beta). \quad (14)$$

In practice, however, the situation is more subtle. For illustration, let us consider the case where the original prior  $\pi(\theta) = \tilde{\pi}(\theta, 1)$  is extremely unrepresentative of the dataset under analysis, so that the original likelihood  $\mathcal{L}(\theta) = \tilde{\mathcal{L}}(\theta, 1)$  is concentrated very far into the wings of  $\pi(\theta)$ . In the limit  $N_{\text{live}} \rightarrow \infty$ , the NS algorithm would nonetheless converge correctly, yielding samples from the posterior (10) and an estimate of the evidence (12). For finite  $N_{\text{live}}$ , however, live points drawn from  $\tilde{\pi}(\theta, \beta)$  at any NS iteration will typically have very low likelihood  $\tilde{\mathcal{L}}(\theta, \beta)$  for values of  $\beta$  above some limiting threshold  $\beta \gtrsim \beta_+$  (which will depend on  $N_{\text{live}}$ ), since the chance of drawing such a live point that lies within the main body of the likelihood  $\tilde{\mathcal{L}}(\theta, \beta)$  is vanishingly small. Depending on the precise nature of the original prior  $\pi(\theta)$  and likelihood  $\mathcal{L}(\theta)$ , a similar phenomenon may also occur for values of  $\beta$  below some other limiting threshold  $\beta \lesssim \beta_-$  (which will also depend on  $N_{\text{live}}$ ).

Thus, in general, one expects NS to produce samples that are drawn not from (10), but from some ‘effective’ posterior

$$\tilde{\mathcal{P}}_{\text{eff}}(\theta, \beta) \propto \mathcal{P}(\theta) \tilde{\mathcal{P}}(\beta), \quad (15)$$

where the marginal posterior  $\tilde{\mathcal{P}}(\beta)$  is (approximately) a top-hat distribution that is non-zero only in the range  $\sim [\beta_-, \beta_+]$ . Hence, by marginalising (15) over  $\beta$  one still obtains the posterior  $\mathcal{P}(\theta)$  on the original parameters. Conversely, marginalising over  $\theta$  one obtains  $\tilde{\mathcal{P}}(\beta)$  and may hence determine the values  $\beta_-$  and  $\beta_+$ , the latter of which is useful in diagnosing the existence and severity of an unrepresentative prior for a given dataset, and thereby identifying the dataset as an ‘outlier’. Here we will take  $\beta_-$  and  $\beta_+$  simply as the smallest and largest  $\beta$  values, respectively, in the set of equally-weighted posterior samples. Alternatively, one could apply some percentile thresholds (e.g. 1% and 99%) to the  $\beta$  marginal, but in practice this leads to very similar values of  $\beta_-$  and  $\beta_+$ . Finally, the NS process will not yield an estimate of the evidence (12), but rather the ‘effective’ evidence

$$\tilde{\mathcal{Z}}_{\text{eff}} \approx (\beta_+ - \beta_-) \tilde{\mathcal{Z}} = (\beta_+ - \beta_-) \mathcal{Z}, \quad (16)$$

from which an estimate of the required evidence  $\mathcal{Z}$  is easily obtained.

## 4 Numerical examples

We now illustrate the performance of the autoPR method in some numerical examples. Since the behaviour of the original PR method has been extensively studied in a wide range of problems by [Chen et al \(2018\)](#), including comparisons with other sampling algorithms such as Markov Chain Monte Carlo (MCMC) and importance sampling, we instead focus here on the performance of the autoPR method in the canonical case where the likelihood and prior on the original variables  $\theta$  are both Gaussian (although very mismatched in some examples), and hence so too is the posterior. In particular, we begin by considering the univariate case, before moving on to a bivariate example for which we consider both circularly-symmetric and asymmetric priors, where the latter may have zero, positive or negative correlation coefficient, respectively. Finally, we investigate higher-dimensional examples, up to 10 dimensions, but consider only circularly-symmetric priors in these cases.

In all our numerical examples, we use the NS package MultiNest ([Feroz et al, 2009](#)), with algorithm parameter settings similar to those used in [Chen et al \(2018\)](#) for the study of the original PR method. Specifically, we set the number of live points  $N_{\text{live}} = 100$ , the sampling efficiency parameter `efr` = 0.8, the convergence tolerance parameter `tol` = 0.5, the multi-modal parameter `mmode` = `False`, and the random seed control parameter `seed` = -1.

### 4.1 Univariate example

We begin by considering a simple one-dimensional estimation problem, for which the data consist of  $N$  independent measurements  $M = \{m_1, \dots, m_n, \dots, m_N\}$  of an unknown parameter  $\theta$ , such that

$$m_n = \theta + \xi, \quad (17)$$

where  $\xi$  denotes Gaussian noise  $\xi \sim \mathcal{N}(\mu_\xi, \sigma_\xi^2)$ . The likelihood is thus given by

$$\mathcal{L}(\theta) = \prod_{n=1}^N \left\{ \frac{1}{\sqrt{2\pi\sigma_\xi^2}} \exp \left[ -\frac{(\theta - m_n)^2}{2\sigma_\xi^2} \right] \right\}, \quad (18)$$

which has a Gaussian form. In particular, we set  $\mu_\xi = 0$ ,  $\sigma_\xi = 1$  and the number of measurements as  $N = 20$ , so that the likelihood is a Gaussian centred around the true value of  $\theta$  with a standard deviation of  $\sim 1/\sqrt{20} \approx 0.22$ . The prior distribution  $\pi(\theta)$  is also assumed to be Gaussian  $\theta \sim \mathcal{N}(\mu_\pi, \sigma_\pi^2)$ , where we set  $\mu_\pi = 0$  and  $\sigma_\pi = 4$ . Therefore one expects *a priori* that the true value of  $\theta$  will lie in the range  $[-12, 12]$  with greater

than 99.5% probability. Finally, we assume the prior distribution of the auxiliary factor  $\beta$  to be the unit uniform distribution  $\beta \sim \mathcal{U}[0, 1]$ .

We consider datasets corresponding to a series of true values  $\theta_*$  ranging between 5 and 50. [Figure 2](#) shows the two limiting examples, corresponding to  $\theta_* = 5$  and  $\theta_* = 50$ , respectively. It is clear that, in the first case, the likelihood is concentrated well within prior distribution's main body (the centre of the likelihood lies at the  $1.25\sigma_\pi$  point of the prior), whereas in the second case the likelihood lies very far into the wings of the prior, which may thus be considered unrepresentative for this data set.

[Figure 3](#) shows the posterior samples obtained in each case using standard MultiNest without PR, together with the corresponding true Gaussian posterior. For the case  $\theta_* = 5$ , it is clear that the MultiNest samples are consistent with the true posterior, but for  $\theta_* = 50$  they differ markedly. The behaviour in the latter case is characteristic of a catastrophic failure mode of the NS algorithm in practice for extreme unrepresentative priors, which is discussed in detail in [Chen et al \(2018\)](#).

This issue may be straightforwardly addressed by applying the proposed autoPR method. [Figure 4](#) shows the resulting MultiNest (with autoPR) joint posterior on  $(\theta, \beta)$  and its marginals for a selection of true values  $\theta_*$  in the range  $[5, 50]$  (the first and last cases, which correspond to those in [Figures 2](#) and [3](#), are plotted in red and purple, respectively). One sees that the joint posterior is precisely of the form expected in [\(15\)](#), in that is the product of two independent distributions on  $\theta$  and  $\beta$ , respectively. One also observes the evolution of the marginal distribution on  $\beta$ . For each value of  $\theta_*$ , this is consistent with a top-hat distribution in the range  $[0, \beta_+]$ , where  $\beta_+$  gradually decreases as  $\theta_*$  increases. For  $\theta_* \lesssim 10$ , one sees that  $\beta_+ \approx 1$ , so one recovers the original uniform prior distribution  $\beta \sim \mathcal{U}[0, 1]$ , indicating that the original prior  $\pi(\theta)$  is representative for these data sets. For  $\theta_* \gtrsim 15$ , however, the value of  $\beta_+$  gradually decreases from unity as  $\theta_*$  increases, which indicates that the original prior  $\pi(\theta)$  is increasingly unrepresentative for these data sets.

Turning to the marginals on  $\theta$  in [Figure 4](#), one sees that they are correctly centred on the mean of the corresponding true Gaussian posterior for every value of  $\theta_*$ . Moreover, the widths of the marginals on  $\theta$  are equal for each value of  $\theta_*$  and consistent with the width of the true Gaussian posterior, hence showing that the autoPR method yields the correct inferences on  $\theta$ , independent of the value of  $\theta_*$ , in a fully automated manner, without any need for tuning. A more quantitative illustration of the parameter estimation accuracy on  $\theta$

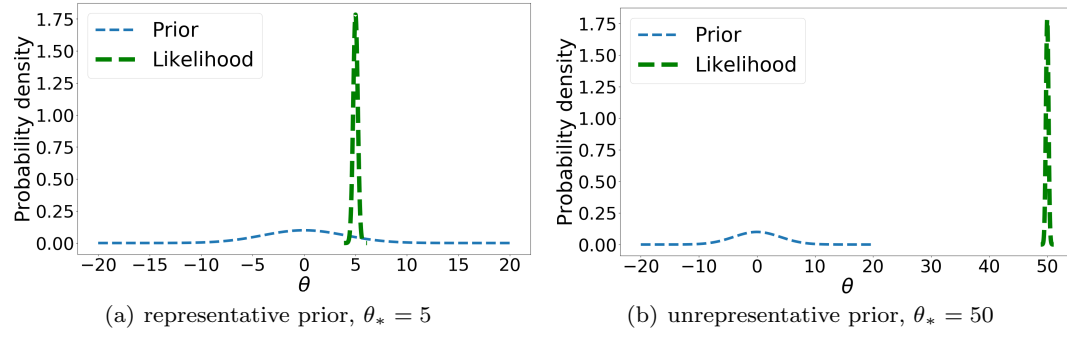


**Fig. 2** Two univariate examples illustrating cases for which the prior is: (a) representative and (b) unrepresentative. The blue and green dashed curves denote the prior and the likelihood, respectively.

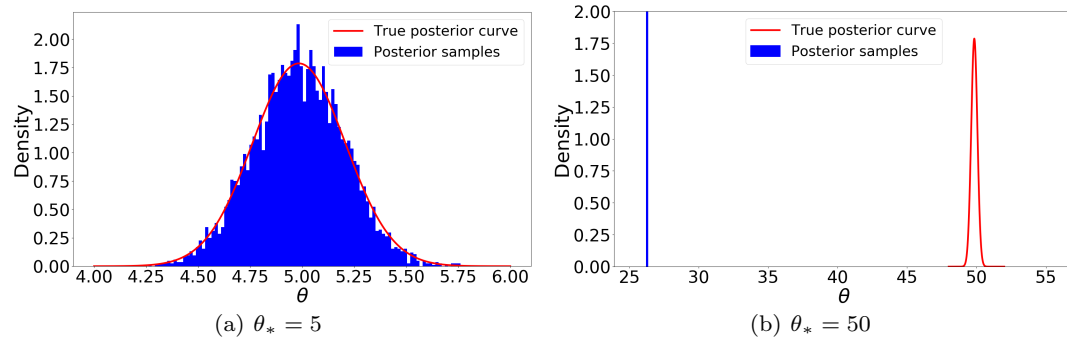


**Fig. 3** Comparison of the posterior samples obtained by standard MultiNest (blue histogram) with the true Gaussian posterior (red curve) for each of the univariate examples plotted in Figure 2.

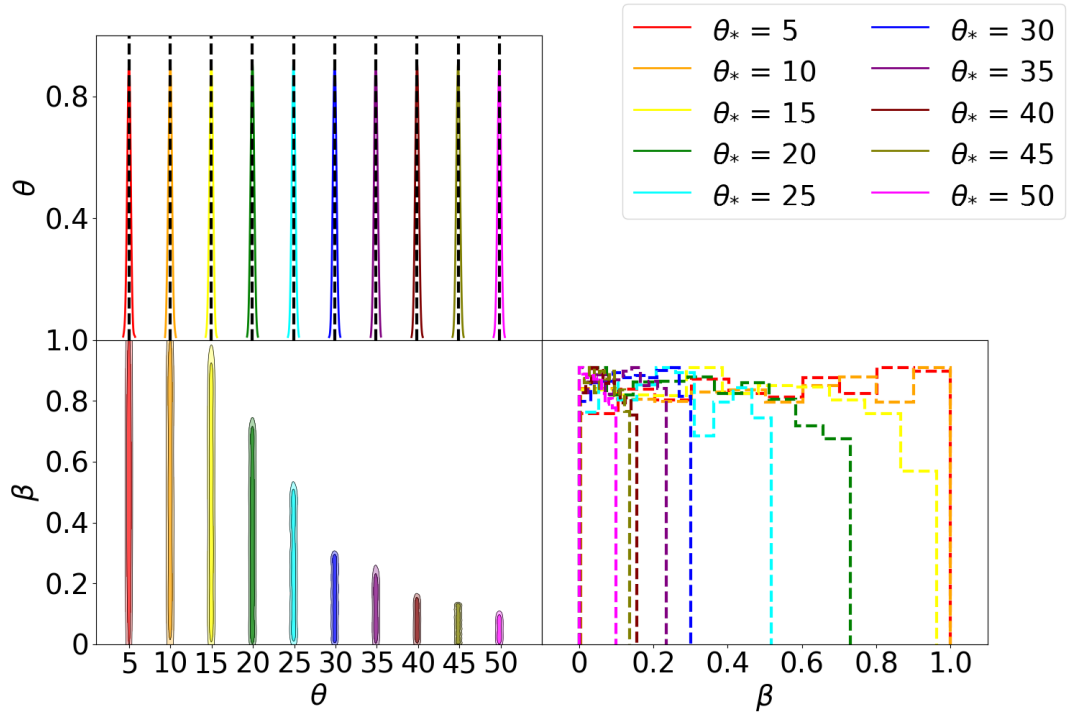


**Fig. 4** A 'corner plot' showing the joint posterior distribution on  $(\theta, \beta)$  obtained by MultiNest using autoPR, together with its marginals, for the univariate example with a range of true values  $\theta_*$ . The vertical dashed black lines in the top left panel indicate true Gaussian posterior in each case.

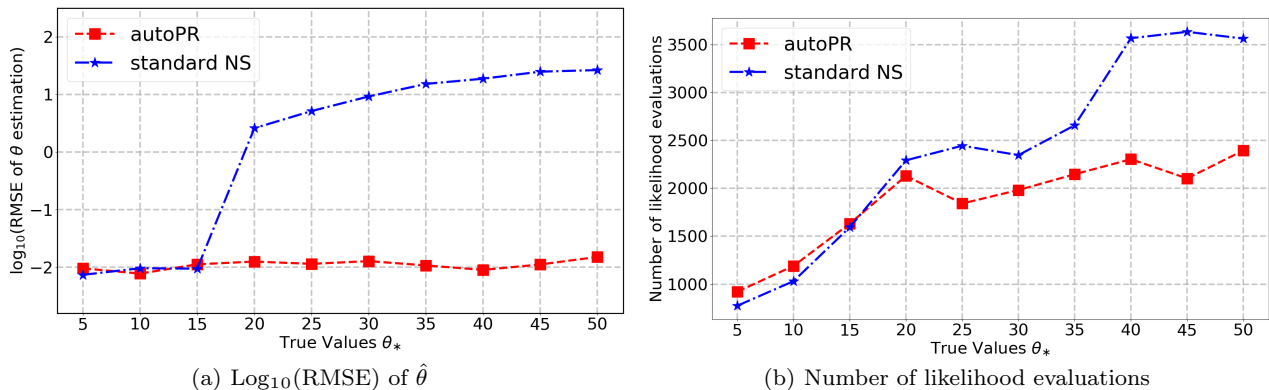


**Fig. 5** Algorithm performance comparison in the univariate example over 10 realisations of the data for each value of  $\theta_*$ . The left panel shows  $\text{Log}_{10}(\text{RMSE})$  of the estimate  $\hat{\theta}$ , and the right panel shows the mean number of likelihood evaluations, both of which are obtained using the standard NS approach (blue star points) and the autoPR method (red square points).

**Table 1** Comparison of the mean and standard deviation of the estimated log-evidence over 10 realisations of the data, obtained using standard NS (SNS) and the autoPR method, for a range of  $\theta_*$  values in the univariate example. The ‘true’ value of the evidence in each case is also given, as estimated using standard quadrature techniques.

$\theta_*$	True	autoPR mean	SNS mean	autoPR s.d.	SNS s.d.
5	-22.0433	-21.9658	-22.0293	0.1793	0.0448
10	-24.3798	-24.1476	-24.8134	0.2073	1.2973
15	-28.2738	-28.0707	-86.7769	0.2433	103.7586
20	-33.7256	-33.6474	-222.5020	0.2663	296.9965
25	-40.7349	-40.5814	-463.2744	0.2722	434.3779
30	-49.3019	-49.3698	-1319.5817	0.2788	1281.9939
35	-59.4265	-59.3564	-2530.0918	0.2929	1631.8255
40	-71.1087	-70.9707	-4309.0312	0.2981	2714.9099
45	-84.3486	-84.2399	-6963.0791	0.3017	3327.0420
50	-99.1461	-99.2356	-10604.4623	0.3102	3816.6693

is given in Figure 5(a), which shows the (logarithm of the) root mean squared error (RMSE) of the estimate  $\hat{\theta}$  over 10 realisations of the data for each value of  $\theta_*$ , for both the standard NS approach and the autoPR method.

One sees that the RMSE of  $\hat{\theta}$  for the standard NS approach rapidly increases for  $\theta_* \gtrsim 20$ , as the prior  $\pi(\theta)$  becomes increasingly unrepresentative and the NS algorithm begins to fail, but that the RMSE of the autoPR method remains stable as  $\theta_*$  increases, indicating robust parameter estimation in all cases. Moreover, for  $\theta_* \lesssim 15$ , the RMSE of the autoPR is consistent with that of the standard NS approach, demonstrating that there is no reduction in estimation accuracy associated with the autoPR method in analysing datasets for which the prior is representative. This is an important conclusion, since it suggests that one sacrifices nothing in terms of parameter estimation accuracy by *always* using the autoPR method, which also has the advantage that one stands to gain considerably from its use when one (unexpectedly) encounters a dataset for which the prior is unrepresentative.

One may also compare the accuracy of the standard NS algorithm and the autoPR method in estimating evidences. Table 1 lists the mean and standard deviation of the estimated log-evidence over 10 realisations of the data for each method, for each considered value of  $\theta_*$ . The table also lists the ‘true’ value of the evidence in each case, estimated using standard quadrature techniques. One sees that for the standard NS approach, the log-evidence estimates quickly become increasingly biased and volatile as  $\theta_*$  increases. By contrast, the log-evidence estimates obtained using autoPR, after making the correction in (16), are all consistent with the true value, and have a standard deviation that remains stable for all values of  $\theta_*$ . This once again suggests that one should *always* using the autoPR method, since the required accuracy in evidence estimation is achieved even for datasets for which the prior is representative.

To demonstrate further the practicality of always using the autoPR method, Figure 5(b) shows the mean number of likelihood evaluations performed by MultiNest over 10 realisations as a function of  $\theta_*$ , for both the standard NS and autoPR methods. One sees that both methods require similar numbers of likelihood evalu-



ations for  $\theta_* \lesssim 20$ , demonstrating that there is very little additional computational overhead resulting from extending the parameter space (in this case doubling its dimensionality) to include the extra hyperparameter  $\beta$ . Moreover, for larger values of  $\theta_*$ , the number of likelihood evaluations required by the standard NS approach continues to increase with  $\theta_*$ , whereas the number required by the autoPR method remains roughly constant. This again suggests that one should use the autoPR method in all applications of NS.

#### 4.2 Bivariate example

We now move to a bivariate example, for which we consider both circularly-symmetric and asymmetric priors, where the latter may have zero, positive or negative correlation coefficient, respectively. In particular, consider a vectorised version of equation (17) from the univariate example, with some  $K = 2$  dimensional parameter vector  $\boldsymbol{\theta} = (\theta_1, \theta_2)^\top$ , such that

$$\mathbf{m}_n = \boldsymbol{\theta} + \boldsymbol{\xi}, \quad (19)$$

where  $\mathbf{m} = (m_1, m_2)^\top$ , and  $\boldsymbol{\xi} = (\xi_1, \xi_2)^\top$  denotes the two dimensional Gaussian noise  $\boldsymbol{\xi} \sim \mathcal{N}(\boldsymbol{\mu}_\xi, \boldsymbol{\Sigma}_\xi)$  with mean  $\boldsymbol{\mu}_\xi$  and covariance  $\boldsymbol{\Sigma}_\xi$ . The prior distribution is also Gaussian,  $\boldsymbol{\theta} \sim \mathcal{N}(\boldsymbol{\mu}_\theta, \boldsymbol{\Sigma}_\theta)$ . We assume unbiased measurements and priors centred on the origin, such that  $\boldsymbol{\mu}_\xi = (0, 0)^\top = \boldsymbol{\mu}_\theta$ , and parameterise the noise and prior covariances matrices by

$$\boldsymbol{\Sigma}_\xi = \begin{bmatrix} \sigma_{\xi_1}^2 & \rho_\xi \sigma_{\xi_1} \sigma_{\xi_2} \\ \rho_\xi \sigma_{\xi_2} \sigma_{\xi_1} & \sigma_{\xi_2}^2 \end{bmatrix},$$

$$\boldsymbol{\Sigma}_\theta = \begin{bmatrix} \sigma_{\theta_1}^2 & \rho_\theta \sigma_{\theta_1} \sigma_{\theta_2} \\ \rho_\theta \sigma_{\theta_2} \sigma_{\theta_1} & \sigma_{\theta_2}^2 \end{bmatrix},$$

where  $\rho_\xi$  and  $\rho_\theta$  are the standard correlation coefficients in each case.

In this example, we take the opposite approach to that used in the univariate example, in that we retain the same likelihood function for each case considered and instead vary the form of the assumed prior, although in all cases the prior is centred on the origin of the parameter space. In particular, we assume throughout the true value  $\boldsymbol{\theta}_* = (40, 40)^\top$ , uncorrelated measurement noise with unit standard deviation, such that  $\rho_\xi = 0$  and  $\sigma_{\xi_1} = \sigma_{\xi_2} = 1$ , and that the number of measurements is just  $N = 1$ , as this yields a circularly-symmetric bivariate Gaussian likelihood distribution of unit standard deviation, which is convenient for our investigations. We present results only for the autoPR method, since the standard NS approach fails in all the cases considered.

##### 4.2.1 Uncorrelated priors

We begin by considering uncorrelated priors, for which  $\rho_\theta = 0$ . In particular, we consider the two circularly-symmetric cases  $\{\sigma_{\theta_1} = 4, \sigma_{\theta_2} = 4\}$  and  $\{\sigma_{\theta_1} = 2, \sigma_{\theta_2} = 2\}$ , and the intermediate non-circularly-symmetric case  $\{\sigma_{\theta_1} = 2, \sigma_{\theta_2} = 4\}$ . These priors and the likelihood are plotted in Figure 6, which illustrates that all the priors are unrepresentative.

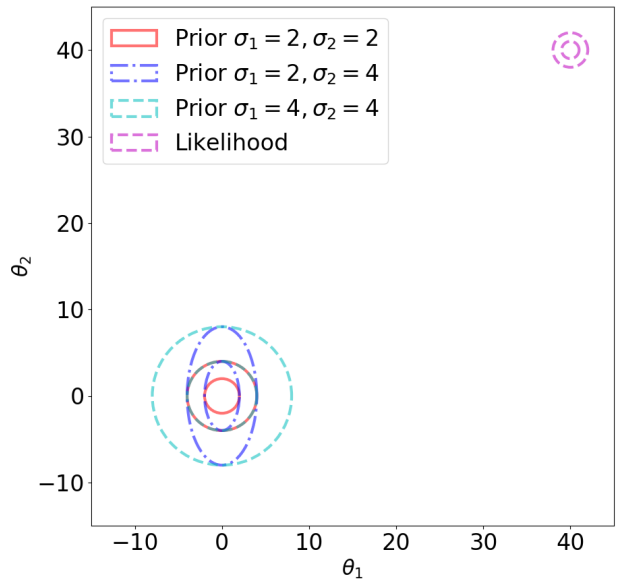


**Fig. 6** Illustration of the three test cases in the bivariate example with uncorrelated priors. The cyan dashed, red solid and blue dot-dashed lines denote the Gaussian priors centred on the origin, with  $\{\sigma_{\theta_1} = 4, \sigma_{\theta_2} = 4\}$ ,  $\{\sigma_{\theta_1} = 2, \sigma_{\theta_2} = 2\}$ , and  $\{\sigma_{\theta_1} = 2, \sigma_{\theta_2} = 4\}$ , respectively. The pink dashed lines in the upper right corner denote the likelihood distribution. Each distribution contains two coloured contours corresponding to the  $2\sigma$  (68%) and  $3\sigma$  (95%) iso-probability levels.

Figure 7 is a ‘corner plot’ showing the 1-dimensional and 2-dimensional marginal distributions of the joint ‘effective’ posterior on  $(\theta_1, \theta_2, \beta)$  for each of the three priors described above. In each case, the joint posterior again has the form of the product of two independent distributions on  $(\theta_1, \theta_2)$  and  $\beta$ , respectively, and is consistent with a marginal on  $\beta$  having the form of a top-hat distribution in the range  $[0, \beta_+]$ . One also observes the expected evolution of this marginal across the three test cases, whereby  $\beta_+$  gradually decreases as the likelihood is concentrated progressively further into the wings of the corresponding prior. Since  $\beta_+ \lesssim 0.1$  in all three cases, one may confirm that each prior is indeed unrepresentative, and one may use the values of  $\beta_+$  for each case to rank their severity.

Turning to the marginals on  $\theta_1$  and  $\theta_2$  in Figure 7, one sees that they are correctly centred on the corre-

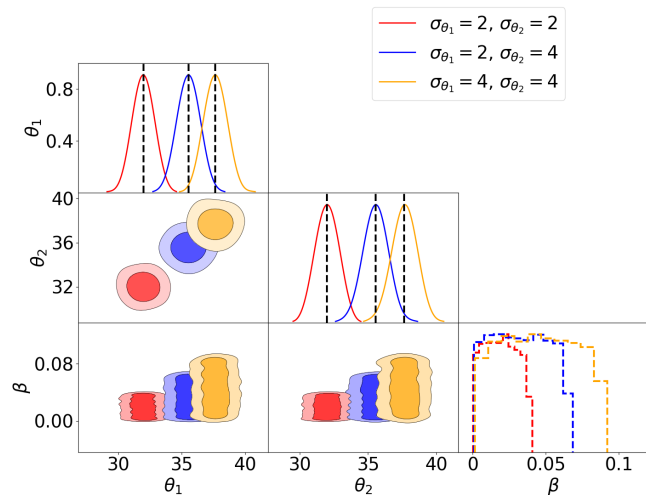


**Fig. 7** A ‘corner plot’ showing the 1-dimensional and 2-dimensional marginals of the joint posterior distribution on  $(\theta_1, \theta_2, \beta)$  obtained by MultiNest using autoPR for the bivariate example with the likelihood and priors illustrated in Figure 6. The vertical dashed black lines indicate the true Gaussian posterior in each case.

sponding true Gaussian posterior for each case. Moreover, the widths of the marginals are stable across the different priors and consistent with the width of the true Gaussian posterior in each case; the RMSE of the  $\theta_*$  estimate  $\approx 0.05$  in all cases. Thus, as in the univariate example, the autoPR method yields the correct inferences on  $(\theta_1, \theta_2)$  without any need for fine tuning.

**Table 2** Comparison of the mean and standard deviation of the estimated log-evidence over 10 realisations of the data in the bivariate example, obtained using standard NS (SNS) and the autoPR method for a selection of uncorrelated priors. The ‘true’ value of the evidence in each case is also given, as estimated using standard quadrature techniques.

Prior	True	autoPR mean	autoPR s.d.
$\{\sigma_{\theta_1} = 4, \sigma_{\theta_2} = 4\}$	-98.7887	-98.5613	0.8808
$\{\sigma_{\theta_1} = 2, \sigma_{\theta_2} = 4\}$	-182.0128	-182.0025	1.2505
$\{\sigma_{\theta_1} = 2, \sigma_{\theta_2} = 2\}$	-325.7575	-325.8910	1.5399

One may also verify that the autoPR method yields accurate evidence estimates in the above cases. Table 2 lists the mean and standard deviation of the estimated log-evidence over 10 realisations of the data for each of the three uncorrelated priors considered; it also lists the corresponding true evidences, estimated using standard quadrature techniques. One sees that in each case the log-evidence estimates obtained using autoPR, after making the correction in (16), are all consistent with the true value, and have a standard deviation that remains stable for all the priors considered.

#### 4.2.2 Correlated priors

We now consider priors with fixed standard deviations  $\{\sigma_{\theta_1} = 4, \sigma_{\theta_2} = 4\}$ , but a range of correlation coefficients  $\rho_\theta = \{-0.75, 0.5, 0.25, 0, 0.25, 0.5, 0.75\}$ . These resulting seven prior distributions are illustrated in Figure 8, together with the likelihood, from which one can see that all the priors are again unrepresentative.

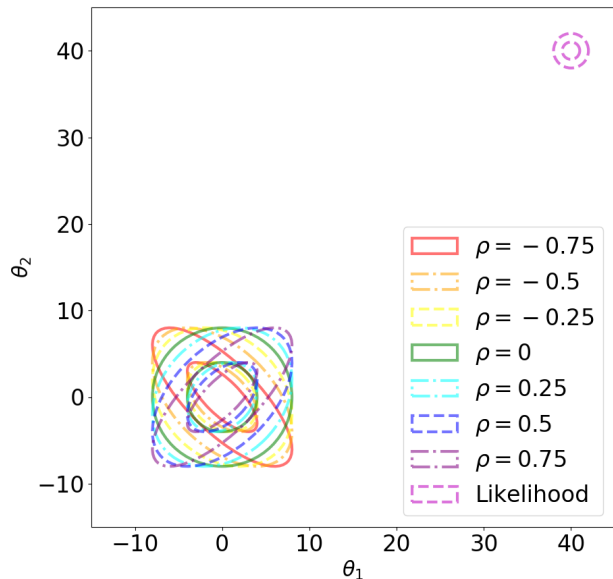


**Fig. 8** Illustration of the seven test cases in the bivariate example with correlated priors, with  $\{\sigma_{\theta_1} = 4, \sigma_{\theta_2} = 4\}$  and correlation coefficients  $\rho_\theta = \{-0.75, 0.5, 0.25, 0, 0.25, 0.5, 0.75\}$ , respectively, denoted in a rainbow colour order. The pink dashed lines in the upper right corner denote the likelihood distribution. Each distribution contains two coloured contours corresponding to the  $2\sigma$  (68%) and  $3\sigma$  (95%) iso-probability levels.

Figure 9 is a ‘corner plot’ showing the 1-dimensional and 2-dimensional marginal distributions of the joint ‘effective’ posterior on  $(\theta_1, \theta_2, \beta)$  for each of the seven priors described above, using the same rainbow colour order as in Figure 8. As in previous examples, the joint posterior in each case has the expected form of the product of two independent distributions on  $(\theta_1, \theta_2)$  and  $\beta$ , respectively, and the marginal on  $\beta$  is consistent with a top-hat distribution in the range  $[0, \beta_+]$ . The evolution of this marginal from  $\rho_\theta = 0.75$  (purple) to  $\rho_\theta = -0.75$  (red) is as expected, with  $\beta_+$  gradually decreasing as the likelihood is concentrated further into the wings of the prior distribution. Moreover, since  $\beta_+ \lesssim 0.15$  in every cases, one may conclude that all the priors are indeed unrepresentative and rank their severity.

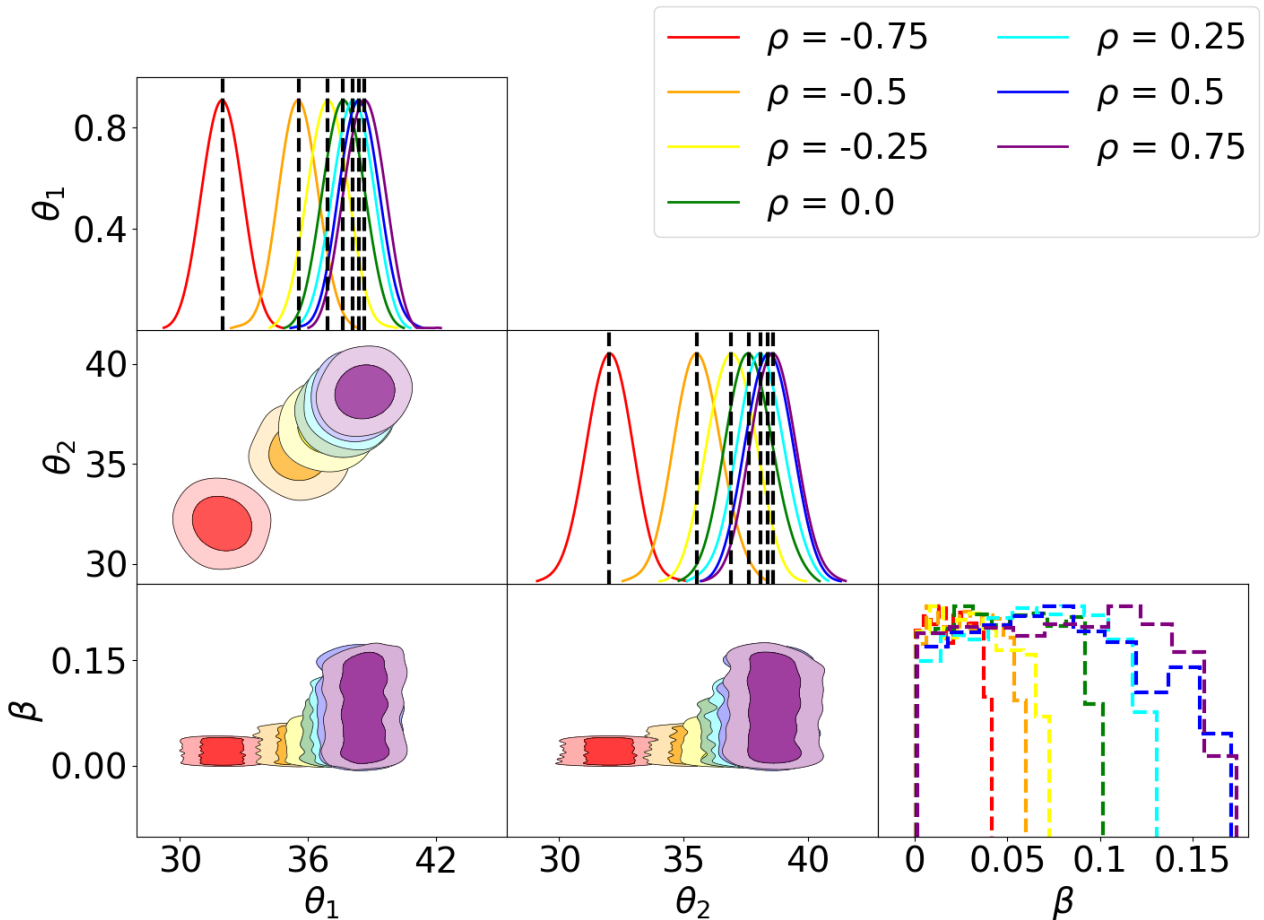


**Fig. 9** A ‘corner plot’ showing the 1-dimensional and 2-dimensional marginals of the joint posterior distribution on  $(\theta_1, \theta_2, \beta)$  obtained by MultiNest using autoPR for the bivariate example with the likelihood and priors illustrated in Figure 8. The vertical dashed black lines indicate the true Gaussian posterior in each case.

The marginals on  $\theta_1$  and  $\theta_2$  in Figure 9 are again correctly centred on the corresponding true Gaussian posterior for each case, which are indicated by the vertical black dashed lines. The widths of the marginals are stable across the range of priors and consistent with the width of the true Gaussian posterior in each case; the RMSE of the  $\theta_*$  estimate  $\approx 0.06$  in all cases. Hence the inferences on the parameters  $(\theta_1, \theta_2)$  using the autoPR method are again accurate and robust in each case, without any tuning.

One may again verify that the autoPR method yields accurate evidence estimates in the above cases. Table 3 lists the mean and standard deviation of the estimated log-evidence values over 10 realisations of the data for each of the seven correlated priors considered, and compares them with the corresponding true evidences estimated using standard quadrature techniques. As for the uncorrelated priors, the log-evidence estimates are all consistent with the true value, and have a stable standard deviation across all the priors considered.

**Table 3** Comparison of the mean and standard deviation of the estimated log-evidence over 10 realisations of the data in the bivariate example, obtained using standard NS (SNS) and the autoPR method for a selection of priors with  $\{\sigma_{\theta_1} = 4, \sigma_{\theta_2} = 4\}$  and correlation coefficient  $\rho_{\theta}$ . The ‘true’ value of the evidence in each case is also given, as estimated using standard quadrature techniques.

$\rho_{\theta}$	True	autoPR mean	autoPR s.d.
-0.75	-324.3385	-324.3237	1.3026
-0.50	-182.3237	-182.4603	1.1131
-0.25	-127.7195	-127.4445	0.7558
0	-98.7887	-98.5232	1.0181
0.25	-80.8330	-80.7149	1.1476
0.50	-68.5459	-68.1668	0.5973
0.75	-59.4986	-59.1786	0.5848

### 4.3 Higher-dimensional examples

We now extend the bivariate example to higher dimensions from 3D to 10D. We begin by adopting an analogous likelihood, corresponding to  $N = 1$  data points and centered on  $\theta_* = 40$  in all dimensions, but restrict

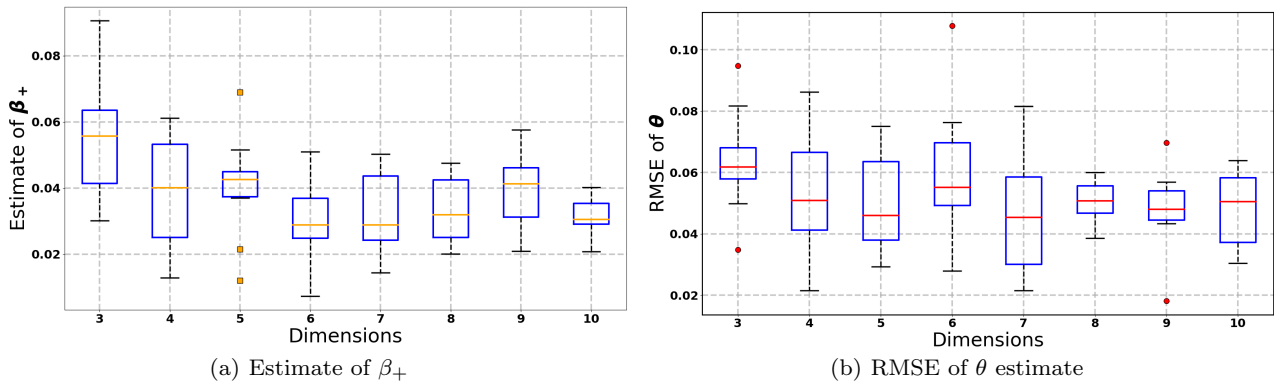


**Fig. 10** Boxplots for parameter estimation results obtained using MultiNest with autoPR in the higher-dimensional examples with  $\theta_* = 40$ , from 3D to 10D. The left plot shows the estimate of  $\beta_+$  and the right plot shows the RMSE on the estimate of  $\theta_*$ . The error bars denote the minimum and maximum values, whereas the boxes indicate the 25th to 75th quantiles. The orange/red line in the box represents the median value over 10 realisations of the data and the points denote outliers.

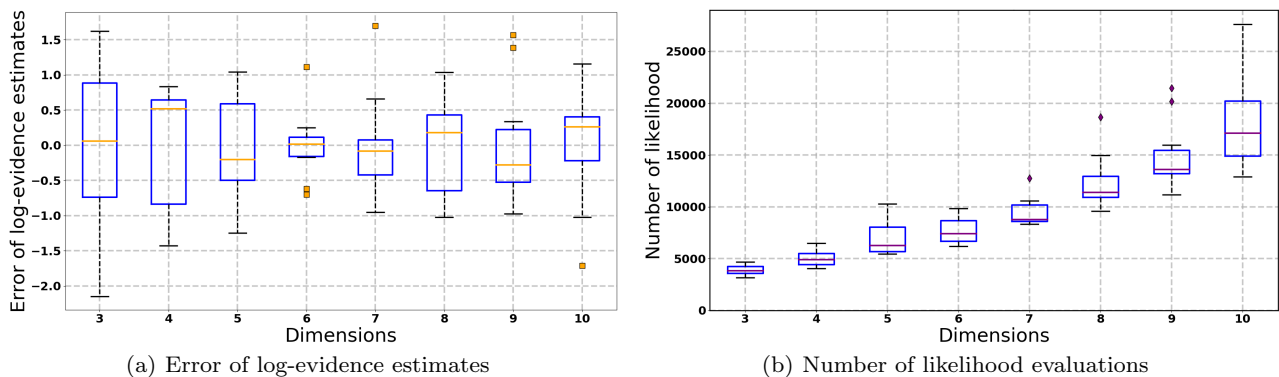


**Fig. 11** Boxplots for (a) error of log-evidence estimation and (b) number of likelihood evaluations required for convergence, obtained using MultiNest with autoPR in the higher-dimensional examples with  $\theta_* = 40$ , from 3D to 10D. The error bars denote the minimum and maximum values, whereas the boxes indicate the 25th to 75th quantiles. The orange/red line in the box represents the median value over 10 realisations of the data and the points denote outliers.

our analysis to the case of a single circular-symmetric Gaussian prior, with  $\sigma_\theta = 4$  in all dimensions. Once again, we consider only the autoPR results as the standard NS method fails completely in this case. All results presented are based on 10 realisations of the data.

We first consider the constraints obtained on the parameters  $(\theta, \beta)$ . Rather than presenting corner plots of the posterior in these higher dimensionalities, Figure 10 instead shows boxplots of the estimated value of  $\beta_+$  (i.e. the upper limit of the top-hat posterior marginal on  $\beta$ ) and the RMSE of the estimate of  $\theta_*$  (averaged across all dimensions), as a function of the dimensionality of the problem. The estimated  $\beta_+$  values are broadly consistent across different dimensionalities, with a mean of  $\approx 0.05$  and standard deviation  $\approx 0.01$ , with only a slight trend to smaller values as the dimensionality increases. This insensitivity to dimensionality is a result of the (effective) joint posterior having the product form (15). Similarly, the RMSE of the  $\theta_*$  estimate is also seen to

be broadly stable across the range of dimensionalities, with a mean value  $\approx 0.05$ , which is consistent with the accuracy obtained in the bivariate example, and standard deviation  $\approx 0.015$ .

Turning to the accuracy of the evidence estimates, Figure 11(a) shows a boxplot of the error in the log-evidence, over 10 realisations of the data, as a function of dimensionality. Once again, one sees that the distributions are relatively stable across different dimensionalities, with errors typically lying within one log-unit, which is consistent with the accuracies achieved in the bivariate example.

Finally, we consider the number of likelihood evaluations  $N_{\text{like}}$  required for MultiNest to converge. Figure 11(b) shows a boxplot of  $N_{\text{like}}$  over 10 realisations of the data, as a function of dimensionality. The mean value of  $N_{\text{like}}$  rises from  $\sim 3800$  at 3D to  $\sim 18100$  at 10D. This trend is consistent with that reported using the original PR method in Chen et al (2018), and follows

roughly an  $\mathcal{O}(n \log n)$  increase with dimensionality. The range of  $N_{\text{like}}$  values over the 10 realisations of the data is also seem to widen slightly as the number of dimensions increases, but this is a relatively minor effect, at least up to 10D.

The above numerical results demonstrate that the autoPR method functions well in higher dimensional problems, with robust performance over multiple experimental realisations, even for the extremely unrepresentative prior considered.

## 5 Conclusions

We have demonstrated that one may straightforwardly automate the prior repartitioning method for improving the robustness and efficiency of nested sampling in the presence of an unrepresentative prior. This is achieved by treating the auxiliary parameter  $\beta$  in the power PR approach as a hyperparameter that is estimated alongside the parameters of interest  $\theta$  of the problem under consideration. Since this estimation process is performed within a single run of the nested sampling algorithm, the autoPR method provides a substantial reduction in the computational requirements relative to the annealing schedule approach adopted in the original PR method. In addition to retaining all the advantages of the original scheme in providing reliable parameter constraints and evidence estimates, the autoPR method adapts automatically to each problem and thus requires no tuning whatsoever. Indeed, by treating  $\beta$  as a hyperparameter, one may use its resulting marginal to determine both the presence and the severity of an unrepresentative prior. We illustrate these properties in a range of numerical examples, from 1D to 10D, with a selection of unrepresentative priors with varying degrees of severity.

Perhaps most interestingly, we show that there is negligible computational overhead relative to standard nested sampling when the autoPR method is used in cases where the prior is representative, and that it offers significant advantages in terms of efficiency and robustness even if the prior is only marginally unrepresentative. This suggests that the autoPR should always be used in the application of nested sampling to Bayesian inference problems, irrespective of whether one suspects that the assumed priors may be unrepresentative for some data sets. This lends the autoPR to being integrated directly into nested sampling algorithms and/or data analysis pipelines.

**Acknowledgements** The authors thank Dr Will Handley and Lukas Tobias Hergt from Cavendish Laboratory at Cam-

bridge University, for their support on the powerful Python visualisation package `anesthetic` (Handley, 2019).

## References

- Chen X, Hobson M, Das S, Gelderblom P (2018) Improving the efficiency and robustness of nested sampling using posterior repartitioning. *Statistics and Computing* pp 1–16 [1](#), [2](#), [4](#), [5](#), [6](#), [12](#)
- Feroz F, Hobson M (2008) Multimodal nested sampling: an efficient and robust alternative to Markov Chain Monte Carlo methods for astronomical data analyses. *Monthly Notices of the Royal Astronomical Society* 384(2):449–463 [2](#)
- Feroz F, Hobson M, Bridges M (2009) MultiNest: an efficient and robust Bayesian inference tool for cosmology and particle physics. *Monthly Notices of the Royal Astronomical Society* 398(4):1601–1614 [2](#), [4](#), [6](#)
- Feroz F, Hobson M, Cameron E, Pettitt A (2013) Importance nested sampling and the MultiNest algorithm. arXiv preprint arXiv:13062144 [4](#)
- Handley W (2019) `anesthetic`: nested sampling visualisation. *The Journal of Open Source Software* 4(37), DOI 10.21105/joss.01414, URL <http://dx.doi.org/10.21105/joss.01414> [13](#)
- Handley W, Hobson M, Lasenby A (2015) POLYCHORD: next-generation nested sampling. *Monthly Notices of the Royal Astronomical Society* 453(4):4384–4398 [2](#), [4](#)
- Higson E, Handley W, Hobson M, Lasenby A (2018) Dynamic nested sampling: an improved algorithm for parameter estimation and evidence calculation. *Statistics and Computing* DOI 10.1007/s11222-018-9844-0, URL <https://doi.org/10.1007/s11222-018-9844-0> [3](#)
- MacKay D (2003) *Information theory, inference and learning algorithms*. Cambridge university press [3](#)
- Skilling J (2006) Nested Sampling for General Bayesian Computation. *Bayesian Analysis* 1(4):833–860 [1](#), [3](#)